Advances in Water Resources 129 (2019) 328–337

Contents lists available at ScienceDirect

Advances in Water Resources

journal homepage: www.elsevier.com/locate/advwatres

Wind effect on gyrotactic micro-organism surfacing in free-surface turbulence

Maryam Mashayekhpour[a,b], Cristian Marchioli[b,*], Salvatore Lovecchio[b], Ebrahim Nemati Lay[a], Alfredo Soldati[b,c]

[a] Department of Chemical Engineering, University of Kashan, 8731753153 Kashan, Iran
[b] Department of Engineering and Architecture, University of Udine, 33100 Udine, Italy
[c] Institute of Fluid Mechanics and Heat Transfer, TU Wien, 1060 Wien, Austria

ARTICLE INFO

Article history:
Received 21 April 2017
Revised 2 September 2017
Accepted 3 September 2017
Available online 13 September 2017

keywords:
Clustering
Free-surface shear flows
Turbulence
Gyrotaxis
Numerical simulation

ABSTRACT

We examine the effect of wind-induced shear on the orientation and distribution of motile micro-swimmers in free-surface turbulence. Winds blowing above the air–water interface can influence the distribution and productivity of motile organisms via the shear generated just below the surface. Swimmer dynamics depend not only on the advection of the fluid but also on external stimuli like nutrient concentration, light, gravity, which are in turn coupled to and influenced by the distribution of the swimmers. Here we focus on gyrotaxis, resulting from the gravitational torque generated by an asymmetric mass distribution within the organism. The combination of such torque with the viscous torque due to shear can reorient swimmers, reducing their vertical migration and causing entrapment in horizontal fluid layers. Through DNS-based Euler–Lagrangian simulations we investigate the effect of wind-induced shear on the motion of gyrotactic swimmers in turbulent open channel flow. We consider different wind forcing and swimmers with different reorientation time (reflecting the ability to react to turbulent fluctuations). We show that only stable (high-gyrotaxis) swimmers may reach the surface and form densely concentrated filaments, the topology of which depends on the wind direction. Otherwise swimmers exhibit weaker vertical fluxes and loose segregation at the surface.

1. Introduction

Wind-induced shear has a profound effect on the transport and mixing processes in the upper layers of large water bodies. In oceans, wind shear affects the vertical distribution and residence time of phytoplankton species rising and sinking across the near-surface region (Enriquez and Taylor, 2015; Moreno-Ostos et al., 2009). In lakes, where water movement is mainly driven by wind, field measurements have shown that strong heterogeneities can be induced in the horizontal concentration distribution (patchiness) of phytoplankton cells (McGillicuddy, 2007; Verhagen, 1994). In the case of shallow productive lakes, wind-induced currents can also influence phytoplankton biomass and composition (Carrick et al., 1993). Motivated by this practical importance, wind-forced physical–biological models that provide statistical estimates of the seasonal phytoplankton cycles in marine ecosystems have been developed (Macías et al., 2012) and simulations aimed at understanding the effect of wind on the physical and/or biological triggers of spring phytoplankton blooms have been performed (Enriquez and Taylor, 2015; McGillicuddy , 2007). One important source of complexity associated with modeling and simulation of plankton interaction with wind-forced fluid turbulence is plankton motility. Many phytoplankton species are self-propelled (Durham et al., 2009; Durham and Stocker, 2012; Guasto et al., 1992) and, even if their swimming speeds are typically smaller than ambient flow speeds, there is well-documented evidence that the interplay between motility and turbulence can result in complex and ecologically important phenomena (Durham et al., 2011; Guasto et al., 1992). In particular, motility can lead to a striking focusing effect known as gyrotaxis when coupled with shear in the form of vertical gradients in horizontal fluid velocity (Guasto et al., 1992; Hoecker-Martínez and Smyth, 2012). Gyrotaxis is the directed motility of cells arising from the combination of gravitaxis (which stabilizes cell orientation in the vertical direction, typically through bottom heaviness) and destabilization by the ambient fluid shear (Durham et al., 2011; 2009; Durham and Stocker, 2012; Kessler, 1986; Pedley and Kessler, 1990; 1992). This results in a balance between the gravitational torque due to the uneven density distribution within the cell, which tends

* Corresponding author.
E-mail address: marchioli@uniud.it (C. Marchioli).

http://dx.doi.org/10.1016/j.advwatres.2017.09.001
0309-1708/

to keep the center of mass below the center of buoyancy, and the hydrodynamic torque exerted by the fluid that surrounds the cell. Gyrotaxis was first observed by showing that phytoplankton cells tend to collect along the centerline of a laminar Poiseuille flow (Kessler, 1986). Subsequent experiments and simulations have demonstrated that gyrotactic plankton can be trapped in horizontal layers in laminar vertical shear (Durham et al., 2009; Ghorai, 2016; Santamaria et al., 2014). Only recently it was discovered that plankton accumulation due to gyrotaxis can occur also in synthetic or homogeneous isotropic turbulence (Croze et al., 2013; De Lillo et al., 2013; 2014; Durham et al., 2013; Santamaria et al., 2014; Thorn and Bearon, 2016; Zhan et al., 2014). In this situation, the resulting spatial distribution is far from uniform and small-scale densely-concentrated clusters with fractal properties are observed (De Lillo et al., 2014; Durham et al., 2013; Fouxon and Leshansky, 2015; Zhan et al., 2014): Gradients in plankton concentration typically span a huge range of length scales, from regions covering thousands of kilometres to patchiness occuring at the scale of centimetres (Dekshenieks et al., 2001; Durham et al., 2009; Steinbuck et al., 2009). Experiments have shown that gyrotactic trapping (Durham et al., 2009; Durham and Stocker, 2012) occurs when vertically-migrating cells reach localized areas of the flow where the vertical gradient of horizontal velocity exceeds a critical shear threshold. This causes cells to tumble end over end, disrupting collective upward motions and preventing any equilibrium orientation from being reached.

To the best of our knowledge, the interplay between wind-induced shear and gyrotaxis in a three-dimensional turbulent flow has never been examined in detail. Therefore, the physical mechanisms that govern the dynamics of motile aquatic micro-organisms (referred to as swimmers hereinafter) in wind-sheared turbulence are not fully understood, and the possibility of observing trapping phenomena in the presence of strong wind-induced shear not yet assessed. Among the few available numerical studies, Enriquez and Taylor (2015) have examined the competition between wind-driven mixing and thermal stratification due to surface heating in triggering spring phytoplankton blooms. To this aim, an Eulerian transport equation with a prescribed depth-dependent growth rate model was used to determine the evolution of plankton concentration. Other processes such as plankton motility and buoyancy were assumed to be too weak to counteract turbulent mixing and, therefore, were not accounted for. Other studies (see De Lillo et al., 2014; Hoecker-Martínez and Smyth, 2012; Manela and Frankel, 2003; Thorn and Bearon, 2016; Zhan et al., 2014 among others) have considered gyrotaxis, yet only in idealized or simplified flow configurations and in the absence of stratification. For instance, Hoecker-Martínez and Smyth (2012) considered a two-dimensional dynamically unstable stratified shear layer (which mimics the surface mixed layer of large water bodies), and found that the resulting pre-turbulent Kelvin-Helmoltz instability is sufficient to enhance the ability of the shear layer to retain gyrotactic organisms. Gyrotactic trapping was also observed by Manela and Frankel (2003) in steady homogeneous shear flow and by Thorn and Bearon (2016) in synthetic turbulence. More recently, Zhan et al. (2014) and De Lillo et al. (2014) investigated the same phenomena considering three-dimensional time-dependent homogeneous isotropic turbulence. Compared to laminar and linear shear flows, clustering and patchiness are significantly reduced but still occur in the downwelling regions of the flow (Zhan et al., 2014). When fluid acceleration is of the same order as gravitational acceleration, however, accumulation phenomena can be enhanced: this condition is unlikely in most marine environments, yet possible under non-homogeneous flow conditions as those encountered in the bottom boundary layer (De Lillo et al., 2014).

In an effort to advance current understanding of how gyrotactic swimmers propel themselves through a wind-sheared fluid, in this paper we investigate their dynamics for the reference case of turbulent open channel flow. In particular, we want to quantify the effect of wind on the vertical migration of swimmers at varying gyrotaxis (covering a wide range of re-orientation times) and at self-propelling speeds that are typical of the most common phytoplankton species. To this aim we use Direct Numerical Simulation (DNS) and Lagrangian Particle Tracking (LPT), modeling swimmers as inertialess pointwise spheres advected by the local fluid velocity while moving with constant self-propelling speed in the direction of their orientation vector. The same methodology has been recently applied to study the surfacing of floaters and the rising of aquatic micro-organisms in free-surface turbulence with and without thermal stratification (Lovecchio et al., 2013; 2017; 2014). In particular, Lovecchio et al. (2013) showed that clusters at the free surface outlive the Eulerian turbulent structures that produced them. This finding was later confirmed by Pratt et al. (2017), and indicates that the instantaneous divergence field alone is not sufficient to capture the formation of the cluster fractal structure and that a Lagrangian approach is needed to capture this long-term clustering. We analyze the effect of different wind directions on surfacing and clustering of the swimmers. We perform this analysis considering swimmers with different bottom-heaviness because this is known to drive different spatial cell distributions, and possibly determine the success of different species in processes like the competition for nutrients and sexual reproduction (Arrieta et al., 2015; Durham et al., 2011). In particular, we take into account the competition between the capability of the swimmers to re-orient themselves against gravity (which favors preferential alignment in the vertical direction and, in turn, surfacing) and the action of the small-scale turbulent fluctuations around the swimmer (which favors tumbling and may hinder surfacing). In the present flow configuration, the effect of wind is reproduced imposing a constant shear stress at the free surface. The paper is organized as follows: The problem statement, the governing equations and the numerical methodology used for the simulations are presented in Section 2; Section 3 is devoted to the analysis and discussion of concentration and orientation statistics, which are used to examine the occurrence of temporary confinement regions for both short and long re-orientation times. Finally, concluding remarks are made in Section 4.

2. Physical problem and methodology

The physical problem considered in this study is the dispersion of gyrotactic swimmers in a wind-sheared turbulent flow in an open channel with a flat undeformable surface (free-surface turbulence). The choice of imposing a flat free surface is based on the findings of several previous studies (Gutiérrez and Aumaître, 2016; Lovecchio et al., 2013; 2014; 2015), which have shown that light particles moving at the deformed free surface of a turbulent flow are subject to clustering mechanisms that come from the horizontal divergence in the surface: These mechanisms induce a compressible effect similar to the one observed for flat surface. In addition, transfer mechanisms across a gas–liquid interface like the one considered in this study are controlled mainly by coherent structures on the liquid side for wind-driven turbulence under the condition of low wind velocity (and no wave breaking) (Takagaki et al., 2016). The reference geometry consists of two horizontal (infinite) flat parallel walls, with the x-, y- and z-axis of the coordinate system pointing in the streamwise, spanwise and wall-normal directions. Indicating with h the channel height, the size of the channel is $2\pi h \times \pi h \times h$ in x, y and z, respectively.

Conservation of mass and momentum of the fluid is described by the following set of three-dimensional time-dependent equations, written in dimensionless vector form:

$$\nabla \cdot \mathbf{u} = 0 \,, \tag{1}$$

$$\frac{\partial \mathbf{u}}{\partial t} + \mathbf{u} \cdot \nabla \mathbf{u} = -\nabla p + \frac{1}{Re_\tau} \nabla^2 \mathbf{u} + \boldsymbol{\delta}_p \tag{2}$$

where $\mathbf{u} = (u_x, u_y, u_z)$ is the fluid velocity, ∇p is the gradient of the fluctuating pressure p, $\boldsymbol{\delta}_p$ is the imposed pressure gradient that drives the flow in the streamwise direction, and $Re_\tau = u_\tau h/\nu$ is the shear Reynolds number based on the shear velocity u_τ, and on the kinematic fluid viscosity $\nu = \mu/\rho$ with μ the fluid kinematic viscosity and ρ the fluid density. The shear velocity is defined as $u_\tau = \sqrt{\tau_w/\rho}$, with τ_w the mean shear stress at the bottom wall in the reference case of no wind forcing acting on the free surface. Based on this definition, $\delta_p = 2\pi\rho u_\tau^2$ in dimensional units. For the fluid velocity, periodic boundary conditions are applied in x and y, whereas no-slip boundary conditions are enforced at the bottom wall ($u_x = u_y = u_z = 0$). At the free surface, a zero vertical velocity (no penetration) boundary condition is imposed in combination with a constant-stress boundary condition, applied to model the wind-induced forcing. In particular, the condition $\tau_{xy}(z = h) = \tau_{wind,+}$ is imposed to simulate the case of wind blowing in the streamwise direction (referred to as co-current wind hereinafter), whereas the condition $\tau_{xy}(z = h) = \tau_{wind,-}$ is imposed to simulate the case of wind blowing against the streamwise direction (referred to as counter-current wind hereinafter).

Eqs. (1) and (2) are discretized using a pseudo-spectral method based on transforming the field variables into the wavenumber space, through a Fourier representation for the periodic (homogeneous) directions x and y, and a Chebychev representation for the wall-normal (non- homogeneous) direction z. A two-level explicit Adams–Bashfort scheme for the non-linear terms and an implicit Crank–Nicolson method for the viscous terms are employed for the time advancement. As commonly done in pseudospectral methods, the convective non-linear terms are first computed in the physical space and then transformed in the wavenumber space using a dealiasing procedure based on the 2/3-rule; derivatives are evaluated directly in the wavenumber space to maintain spectral accuracy. Further details can be found in Lovecchio et al. (2013).

Individual swimmers are modeled as spherical particles whose position $\mathbf{x}_p$ evolves in time according to the following equation:

$$\dot{\mathbf{x}}_p(t) = \mathbf{u}_{@p}(\mathbf{x}_p, t) + v_s \mathbf{p}, \tag{3}$$

where v_s is the (constant) swimming speed, $\mathbf{u}_{@p}(\mathbf{x}_p, t)$ the velocity of fluid in the position of swimmer and $\mathbf{p}$ defines the spatial orientation of the swimmer. The orientation vector $\mathbf{p}$ evolves in time according to the response of the swimmer to the biasing torques acting upon it: The viscous torque on the swimmer body, caused by the local shear, and the gyrotactic torque, arising from bottom heaviness (Pedley and Kessler, 1992) (see Fig. 1). For spherical inertialess swimmers, the orientation rate is computed from the following equation (Voth and Soldati, 2017):

$$\frac{\mathrm{d}\mathbf{p}}{\mathrm{d}t} = \frac{1}{2B}[\mathbf{k} - (\mathbf{k} \cdot \mathbf{p})\mathbf{p}] + \frac{1}{2}\boldsymbol{\omega}_{@p} \wedge \mathbf{p} \tag{4}$$

where $\mathbf{k} = [0, 0, 1]$ is a unit vector pointing upward in the vertical direction, $\boldsymbol{\omega}_{@p}$ is the fluid vorticity at the swimmer's position and $\mathcal{B}$ is the characteristic time a perturbed gyrotactic swimmer takes to return to the vertical orientation when $\boldsymbol{\omega}_{@\mathbf{p}} = 0$. Such reorientation time can be computed as $\mathcal{B} = \mu\alpha_\perp/(2\mathcal{H}\rho g)$, where $\alpha_\perp$ is the dimensionless resistance coefficient for rotation about an axis perpendicular to $\mathbf{p}$ and $\mathcal{H}$ is the center-of-mass offset relative to the center of buoyancy (located at point B in Fig. 1).

The first term on the right hand side of Eq. (4) represents the tendency of a swimmer to remain aligned with the vertical direction due to bottom-heaviness, while the second term represents the tendency of fluid vorticity to overturn the swimmer through a viscous torque. The time evolution of swimmer's position and orientation were computed upon time integration of the

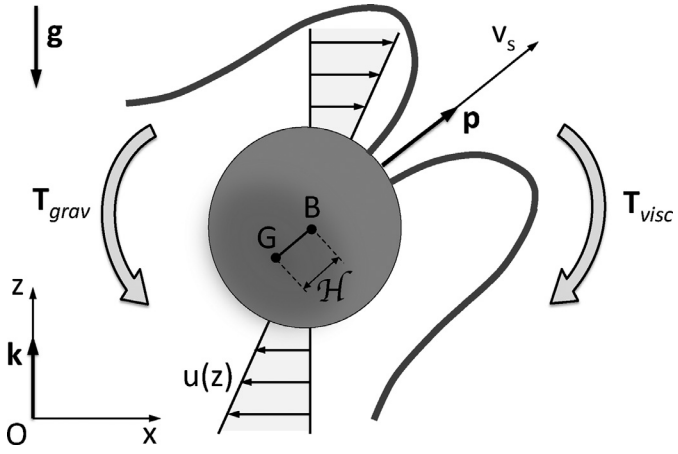

Fig. 1. Gyrotactic micro-organisms swim with velocity v_s in the direction given by the orientation vector $\mathbf{p}$, set by a balance of torques: the torque due cell asymmetry (bottom heaviness: $\mathbf{T}_{grav}$), which tends to align the cell to its preferential orientation along the vertical direction $\mathbf{k}$, and the torque due to flow ($\mathbf{T}_{visc}$), which tends to rotate the cell according to the local velocity gradients.

non-dimensional form of Eqs. (3) and (4), which read as:

$$\frac{\mathrm{d}\mathbf{x}^+_{@p}}{\mathrm{d}t^+} = \mathbf{u}^+_{@p}(\mathbf{x}^+_{@p}, t^+) + \Phi\mathbf{p}, \tag{5}$$

$$\frac{\mathrm{d}\mathbf{p}}{\mathrm{d}t^+} = \Psi[\mathbf{k} - (\mathbf{k} \cdot \mathbf{p})\mathbf{p}] + \frac{1}{2}\boldsymbol{\omega}^+_{@p} \wedge \mathbf{p} \tag{6}$$

where superscript + represents dimensionless variables in wall units, obtained using u_τ and ν. The key parameters in Eqs. (5) and (6) are the swimming number $\Phi = v_s/u_\tau$ and the stability number $\Psi = \frac{1}{2\mathcal{B}}\frac{\nu}{u_\tau^2}$, which parameterises the importance of vortical overturning with respect to directional swimming. Time integration exploits a fourth-order Adams–Bashforth scheme, starting from a two-dimensional random distribution (in both space and orientation) of 10^6 Lagrangian swimmers at the centerplane of the channel. Swimmers are tracked using a point-particle approach, justified by the sub-Kolmogorov size typical of aquatic microorganisms, and are injected into the flow at a concentration low enough to consider dilute conditions: the effect of the swimmers on turbulence is neglected (one-way coupling) as well as collisions between swimmers. Periodic boundary conditions are imposed on swimmers moving outside the computational domain in the horizontal (homogeneous) directions. In the wall-normal direction, the swimmers rebound elastically at both boundaries. The assumption of fully elastic rebound to describe particle interaction with a free surface might not be obvious. Indeed the proper numerical modeling of particle rebound at a free surface is an issue that has been little explored in the literature: As far as point-particle Euler–Lagrange simulations in open channel flow are concerned, we are only aware of the study by Chidambaran et al. (2003), where the free surface was treated as a perfectly absorbing boundary. In the present study, we have decided to impose an elastic rebound because, differently from inelastic rebound or absorbing wall, it does not enhance "artificially" particle trapping at the free surface: Hence, this boundary condition is the most conservative as far as surfacing is concerned. In addition, it appears reasonable in view of the fact that swimmers see the free surface as a non-deformable boundary. We also remark that any other choice of boundary condition would have imposed a constraint on particle dynamics. A perfectly absorbing free-surface would have required re-initialization of the absorbed particle to keep the total number of particles constant in time: This way, however, the velocities of the reintroduced particles would have been affected by the

Table 1
Summary of the simulation parameters.

Simulation	Ψ	Re_τ	Φ	$\tau^+_{wind,\pm}$
S0.1	0.0113			
S0.2	0.113	171	0.048	0
S0.3	1.13			
S1.1	0.0113			
S1.2	0.113	171	0.048	+0.7
S1.3	1.13			
S2.1	0.0113			
S2.2	0.113	171	0.048	-0.35
S2.3	1.13			

imposed initial condition for a certain amount of time. An inelastic rebound would have required to select the value of the restitution coefficient, which accounts for the amount of energy dissipated during the contact: To the best of our knowledge, this problem has never been investigated and, therefore, the only option one is left with is to pick an arbitrary value.

The fluid velocity and vorticity at the instantaneous location of the swimmer is obtained through interpolation based on 6th-order Lagrange polynomials.

A campaign of direct numerical simulations, summarized in Table 1, was performed to investigate the role of wind-induced shear on the motion of the swimmers. All simulations were run at reference Reynolds number $Re_\tau = 171$, with spatial grid resolution of $128 \times 128 \times 129$ points. Grid points are uniformly distributed in the horizontal directions x and y, and the corresponding grid spacings are $\Delta x^+ \simeq 8.4$ and $\Delta y^+ \simeq 4.2$. In the wall-normal direction, a non-uniform distribution of nodes based on Chebychev polynomials has been used, and the grid spacing varies from $\Delta z^+ = 0.025$ near the vertical boundaries to $\Delta z^+ \simeq 2.12$ in the domain center. Considering that the Kolmogorov length scale in the flow ranges from $\eta_K^+ \simeq 1.6$ at the bottom wall to $\eta_K^+ \simeq 3.6$ at the free surface, this resolution appears sufficient to solve for all flow scales. As shown by Nagaosa (1999), Nagaosa and Hadler (2003) and Calmet and Magnaudet (2003), the structure of the turbulent flow that characterizes the free-surface at Reynolds numbers comparable to the one considered in the present study is strongly connected to the bursting phenomena that occur near the bottom wall. The imposed wind stress was set equal to $\tau_{wind,+} = 0.006$ Pa (0.7 in wall units) for the counter-current wind simulations, indicated as S1.# in Table 1, and to $\tau_{wind,-} = -0.003$ Pa (-0.35 in wall units) for the co-current wind simulations, indicated as S2.# in Table 1. These values correspond to a mild wind speed of about 1.5 m/s at a reference altitude of 10 m (Yelland and Taylor, 1996). Based on the experimental findings of Walker and Peirson (2008), such wind speed does not generate any wave motion at an air–water interface. Present results thus apply to gas–liquid interfaces that are free of impurities or surfactants, and to situations in which surface tension and gravity are sufficiently strong (namely the Froude and Weber numbers are sufficiently small) to damp the vertical liquid motions at the surface. We also remark that the restriction to a non-deformable free surface and a uniform wind stress excludes processes such as wave breaking and Langmuir circulations (Kramer et al., 2010). To relate the two forces driving the flow, i.e. the pressure gradient and the free-surface stress, the ratio $\mathcal{R}_\tau = \tau_{wind,\pm}/\tau_{wall}$ between the applied surface stress and the maximum stress observed at the bottom, τ_{wall}, can be used. In the present simulations, wind forcing yields $\mathcal{R}_\tau \simeq 0.3$. Clearly, $\mathcal{R}_\tau = 0$ with no forcing. To simulate the motion of the microorganisms, we considered a fixed value of the swimming number ($\Phi = 0.048$), corresponding to a dimensional swimming velocity $v_s = 100$ μ m/s typical of *Chlamydomonas augustae* cells (Croze et al., 2013; Durham et al., 2013), but three different values of the stability number ($\Psi_H = 1.13$, $\Psi_I = 0.113$, $\Psi_L = 0.0113$), corresponding to $\mathcal{B} = 0.054, 0.54$ and 5.4 s, respectively: These values fall within the typical range of motile phytoplankton species (0.1 $s < B < 10$ s). We remark here that, in the present flow configuration, the Kolmogorov timescale varies from $\tau^+_{K,min} \simeq 2$ at the wall to $\tau^+_{K,max} \simeq 13$ at the free-surface (Lovecchio et al., 2013). Therefore, the selected values of the stability number correspond to three different physical instances with respect to $\tau^+_{K,max}$. At one extreme, $\Psi_L \cdot \tau^+_{K,max} \sim \mathcal{O}(10^{-1})$ represents the case in which the timescale of gravitaxis is large compared to the timescale of the dissipative surface eddies and so the directional motion of the swimmers is dominated by the destabilizing effect of small-scale turbulence throughout the channel. At the opposite extreme, $\Psi_H \cdot \tau^+_{K,max} \sim \mathcal{O}(10)$ represents the case in which the timescale of gravitaxis is small compared to the timescale of the dissipative surface eddies and so the directional motion of the swimmers is dominated by the stabilizing effect of bottom heaviness. The intermediate case $\Psi_I \cdot \tau^+_{K,max} \sim \mathcal{O}(1)$ represents the situation in which the two timescales are comparable and so the motion of the swimmers results from the competition between small-scale turbulence around each cell and bottom heaviness.

3. Results and discussion

In this section, we discuss first the statistical features of the velocity field in the presence of wind forcing at the surface. Then, we examine the effects of such turbulent flow on plankton surfacing, in terms of preferential segregation (patchiness), vertical concentration and orientation distribution.

3.1. Statistical characterization of the flow field

We start our analysis by considering how the wind-induced shear influences the mean flow field in the open channel. In Fig. 2(a) the mean streamwise velocity profile $\langle u_x^+ \rangle$ (in wall units) is shown for the different wind directions as a function of the wall-normal distance from the free surface, $Z^+ \equiv z^+ - Re_\tau$. Brackets indicate time and space average. The averaging procedure is the same adopted in Lovecchio et al. (2014) and is based on snapshots of the velocity field separated in time exceeding the correlation time and in space exceeding the integral scale. A boundary layer is present at the no-slip bottom, where the fluid velocity is reduced to zero with different slope depending on the type of wind forcing applied. In the free-surface layer, the velocity adapts to the value at the surface, which is $\langle u_x^+ \rangle_{surf} \simeq 24.8$ in the co-current wind case and $\langle u_x^+ \rangle_{surf} \simeq 18.4$ in the counter-current wind case (compared to a value $\langle u_x^+ \rangle_{surf} \simeq 14.1$ in the free-surface case). In Fig. 2(b) we show the corresponding mean shear, $\langle \mathrm{d}u_x^+/\mathrm{d}z^+ \rangle$, which reaches its maximum value at the bottom wall. Note that the value of this maximum changes among the different simulations. Due to wind forcing, the wall shear stress in the co-current case increases with respect to the free-slip simulation, whereas the wall shear stress in the counter-current case decreases. Changes of the wall shear stress correspond to changes of the shear velocity and, in turn, of the shear Reynolds number because the overall force balance on the channel is affected. Elaborating, in the co-current (resp. counter-current) case the effect of wind on the fluid at $Re_\tau = 171$ is to generate the same fluid statistics that would be obtained in a simulation without wind forcing at suitably higher (resp. lower) shear Reynolds number. Flow field statistics in the different wind configurations must thus be examined taking this effect into account.

Another important feature of $\langle \mathrm{d}u_x^+/\mathrm{d}z^+ \rangle$ is that a local peak of shear is reached at the free-surface when wind forcing is applied. A similar situation is observed in the case of stably-stratified

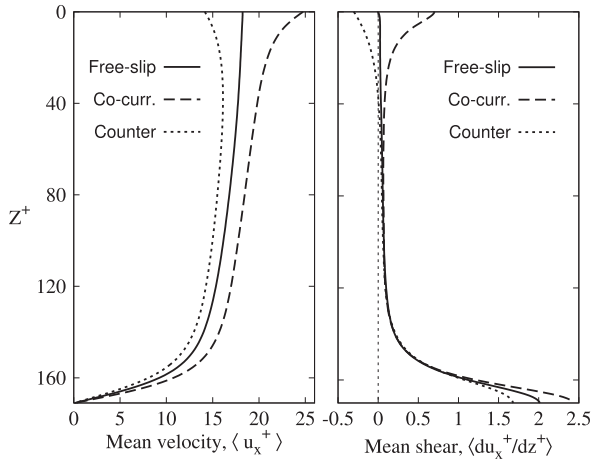

Fig. 2. Mean streamwise fluid velocity (a) and mean vertical fluid shear and (b) in wind-sheared free-surface turbulence. The free surface is located at $Z^+ = 0$. Lines correspond to different wind conditions at the free-surface: Free-slip surface (solid line); co-current wind (dashed line); counter-current wind (dotted line).

turbulent flow, where strong shear is generated below the free surface, in regions of large temperature gradients and low mixing (thermoclines) (Lovecchio et al., 2017). Our aim is precisely to quantify the effect of such shear on the vertical migration and surfacing of the swimmers in a situation of competition between gravitaxis (which tends to preferentially orient the swimmers in the vertical direction) and the ambient fluid shear (which tends to randomize cell orientation).

To observe the influence of wind on mixing and turbulence characteristics, in Fig. 3 we examine the root mean square (rms) of the fluid velocity fluctuations in each direction. When no wind forcing is applied (solid lines), the velocity fluctuations near the bottom wall (where turbulence production is maximum) are similar to those observed in standard closed channel simulations, indicating that the near-wall turbulence is not influenced by the presence of a free-slip top boundary (Lovecchio et al., 2014). The most evident difference associated to the presence of the free surface is that $\langle rms(u_x^+)\rangle$ and $\langle rms(u_y^+)\rangle$ are not zero at the surface itself, where $\langle rms(u_z^+)\rangle$ is bound to vanish thus making turbulence nearly two-dimensional in a tiny sub-surface layer. When wind forcing is applied along the mean flow direction (dashed lines), all rms components increase significantly throughout the channel, with the exception of the very-near wall region (confined within a distance $z^+ \simeq 10$ from the bottom), where the typical dynamics of the wall turbulence is maintained. This behavior is related to the increase of wall shear stress and shear velocity observed in the co-current case. The increase of velocity fluctuations in the horizontal directions persists up to the free surface, where $\langle rms(u_z^+)\rangle$ is less influenced owing to the strong constraint on u_z' imposed by the assumption of undeformable free surface. When wind forcing is applied against the mean flow direction (dotted lines), a general decrease of velocity fluctuations is found, with a slightly weaker effect observed for $\langle rms(u_x^+)\rangle$. This behavior is related to the decrease of wall shear stress and shear velocity observed in the counter-current case. Therefore, counter-current wind forcing reduces agitation due to turbulence and has a stabilizing effect on the flow field. Because the characteristic timescale of turbulent advection along the vertical direction is much shorter (one order of magnitude at least) than the timescale of self-propelling advection, the observed changes of velocity fluctuations have a non negligible impact on the vertical motion of gyrotactic swimmers and on their capability to reach the surface.

3.2. Characterization of plankton clustering through surface divergence

Planktonic swimmers are initially positioned midway between the bottom wall and the free surface ($z/h = 0.5$), with random orientation. Due to gravitaxis, swimmers tend to rise towards the free surface. Once there, helped by the reduction of wall-normal velocity fluctuations, gravitaxis further acts to keep the cells at the surface. In this region of the flow, swimmer dynamics is closely related to the local structure of the velocity field (Lovecchio et al., 2013; 2014). For the flow Reynolds number considered in this study, turbulence at the free surface is nearly two dimensional, with surface structures generated and sustained by bursting phenomena that are continuously produced by wall-shear turbulence inside the buffer layer (Calmet and Magnaudet, 2003; Nagaosa, 1999; Nagaosa and Hadler, 2003). The correlation between free-surface structures and bursting phenomena is known to weaken as the flow Reynolds number increases (Calmet and Magnaudet, 2003). Two-dimensional turbulence can be characterized by the divergence of the velocity field:

$$\nabla_{2D} = \frac{\partial u}{\partial x} + \frac{\partial v}{\partial y} = -\frac{\partial w}{\partial z} \,. \tag{7}$$

In the present flow configuration, ∇_{2D} does not vanish at the free surface (Cressman et al., 2004). Therefore plankton cells probe a compressible two-dimensional system (Lovecchio et al., 2013), where velocity sources are regions of local flow expansion ($\nabla_{2D} > 0$) generated by sub-surface upwellings and velocity sinks are regions of local compression ($\nabla_{2D} < 0$) due to downwellings (Cressman et al., 2004). In Fig. 4 we provide a qualitative characterization of plankton clustering on the free surface by correlating the instantaneous particle patterns with the colormap of ∇_{2D}: strong velocity sources are visualised in red, strong velocity sinks are visualised in blue. All flow configurations and all gyrotaxis levels are considered in this figure. As shown by Lovecchio et al. (2013); 2017); 2014), a general behavior, common to all cases we examined, is that plankton cells reach the surface mainly through velocity sources and subsequently collect into velocity sinks. Once trapped in these regions, swimmers organize themselves in clusters that are stretched by the fluid forming filamentary structures. Eventually sharp patches of plankton density distribution are produced, which correlate very well with the rapidly changing patches of ∇_{2D}, as shown by Fig. 4. Similar behavior (the formation of clusters with fractal mass distribution) has been observed for the case of floaters in surface flow turbulence, both with Lovecchio et al. (2014) and without mean shear (Lovecchio et al., 2013).

Fig. 4 demonstrates clearly that the topology of the velocity sources/sinks and the fractal dimension of the plankton clusters are both dependent on the wind forcing and on gyrotaxis. In the reference case of free-surface flow with no wind forcing (top panels in Fig. 4), we observe a clear and rather sharp alternation of sources and sinks, flanked by densely-populated clusters forming only for high enough gyrotaxis (corresponding to stability numbers equal to or larger than Ψ_I, in our simulations). If gyrotaxis is low, as in panel 4(a), then only very few cells can reach the surface and no evident cluster is formed. In the co-current wind case (middle-row panels in Fig. 4), we observe a sharper alternation of velocity sources and sinks, which appear to be characterized by smaller spatial extent. This is in agreement with the increase of velocity fluctuations in the horizontal directions discussed previously. Clusters form only in the case of very high gyrotaxis (Fig. 4f), indicating that plankton cells need strong vertical stability to overcome the wind-induced shear barrier and reach the surface. Compared to the no-wind case with $\Psi = \Psi_H$ (Fig. 4c), clustered filaments appear to be more concentrated and aligned with the mean flow direction.

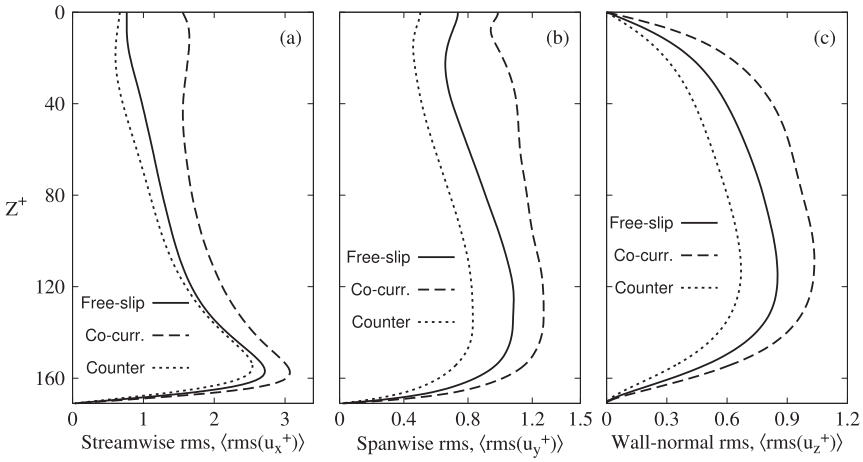

Fig. 3. Root mean square (rms) of fluid velocity: (a) streamwise component; (b) spanwise component and (c) wall-normal component. The surface is located at $Z^+ = 0$. Lines are as in Fig. 2.

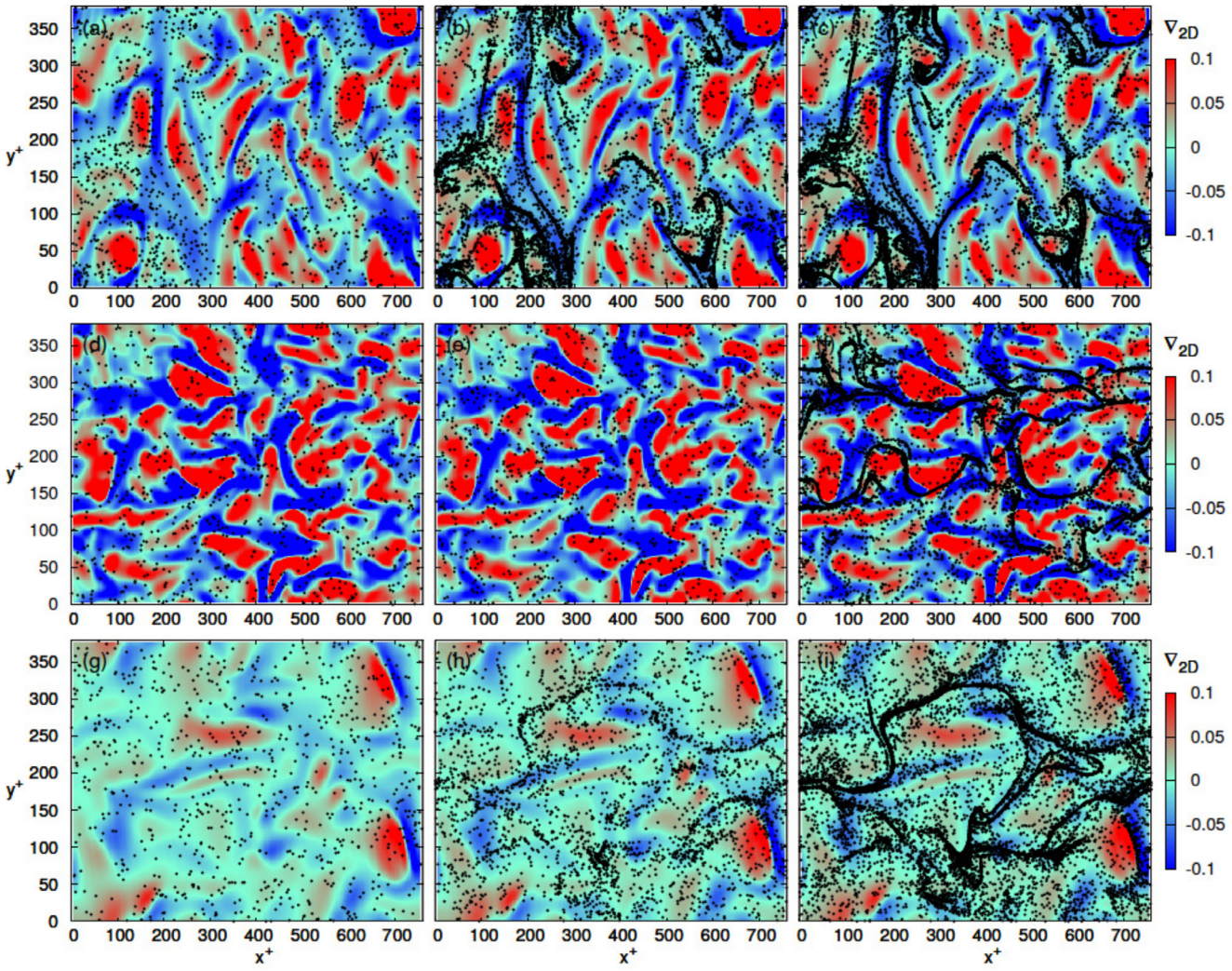

Fig. 4. Surface divergence and instantaneous particle distribution for the different flow configurations. Top row: free-slip surface (base simulation); middle row: co-current wind; bottom row: counter-current wind. Left-hand column: low gyrotaxis, Ψ_L; central column: intermediate gyrotaxis, Ψ_I; right-hand column: high gyrotaxis, Ψ_H. (For interpretation of the references to color in this figure, the reader is referred to the web version of this article).

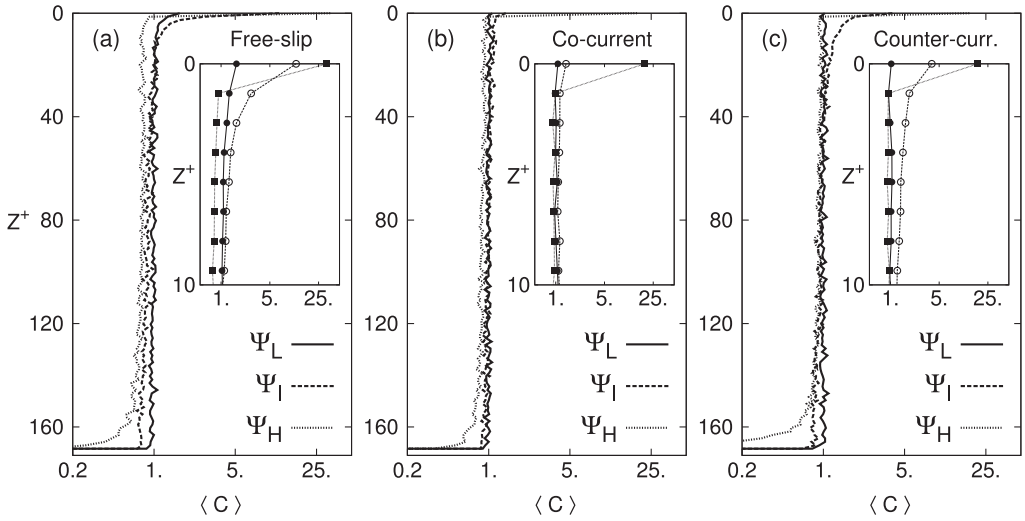

Fig. 5. Instantaneous concentration profiles at $t^+ \simeq 2000$ in the vertical direction. Panels: (a) free-slip surface; (b) co-current wind and (c) counter-current wind. The free surface is located at $Z^+ = 0$. The inset in each panel shows a close-up view of concentration within a distance of 10 wall units from the free-surface. Lines: low gyrotaxis, Ψ_L (solid lines); intermediate gyrotaxis, Ψ_I (dashed lines); high gyrotaxis, Ψ_H (dotted lines). Symbols in the insets: Ψ_L (•); Ψ_I (○); Ψ_H (■).

In the counter-current wind case (bottom-row panels in Fig. 4), we observe a strikingly different flow topology: Surface flow structures more rarely appear in the form of strong sources/sinks, in agreement with the observed decrease of velocity fluctuations on the surface plane. Clusters start forming already at intermediate gyrotaxis ($\Psi = \Psi_I$, Fig. 4h), yet become evident only in the high gyrotaxis case ($\Psi = \Psi_H$, Fig. 4i). Indeed, compared to the co-current case, the counter-current wind generates lower shear in the near-surface layers, which can thus be reached also by cells with intermediate vertical stability. Compared to the Ψ_H case with no wind forcing (Fig. 4c), clustered filaments appear again more aligned with the mean flow direction.

3.3. Characterization of plankton surfacing

The different clustering dynamics discussed in Fig. 4 provide qualitative evidence of significant wind effects on the capability of motile organisms to migrate vertically and reach the surface. To quantify this effect, we examine next the instantaneous swimmer concentration, $C(z)$, along the vertical direction. The concentration $C(z)$ represents a volumetric number density and has been obtained by coarse-graining the instantaneous vertical position of the swimmers on horizontal fluid slabs. This observable is shown in Fig. 5, at the end of the simulation (namely at time $t^+ \simeq 2000$ after injection of the plankton cells into the turbulent flow) and for all cases simulated in the ($\mathcal{R}_\tau$, Ψ) parameter space. Each profile in Fig. 5 corresponds to a specific level of gyrotaxis. The inset in each panel provides a close-up view of the different concentration profiles below the free surface: For ease of reading, symbols have been added to lines.

In the free-slip case (Fig. 5a), concentration builds up within a thin layer just below the surface. The maximum value of concentration is reached right at the surface, and increases monotonically with gyrotaxis. In the bulk of the flow, the distribution of the swimmers remains uniform whereas the bottom wall is depleted of cells, indicating a continuous steady migration towards the free-surface. In the co-current case (Fig. 5b), it can be observed that wind-induced shear prevents the formation of the concentration peak unless the vertical stability of the swimmers is high (as indicated by the black squares in the inset of Fig. 5b). Accumulation is prohibited when swimmers react slowly to external fluid velocity fluctuations and gradients. Similar considerations can be made for the counter-current case (Fig. 5c), noting that wind-induced shear is lower compared to the co-current case and, therefore, a detectable concentration peak can develop also at Ψ_I. A general conclusion that can be drawn from Fig. 5 is that, differently from the case of steady shear flows or homogeneous isotropic turbulent flows (De Lillo et al., 2014; Durham et al., 2009; Fouxon and Leshansky, 2015; Ghorai, 2016; Hoecker-Martínez and Smyth, 2012; Manela and Frankel, 2003; Santamaria et al., 2014; Thorn and Bearon, 2016; Zhan et al., 2014), no gyrotactic trapping occurs and local peaks of concentration do not develop below the high-shear layers below the surface. This happens because the characteristic timescale of turbulent advection along the vertical direction is much shorter (one order of magnitude at least) than the timescale of self-propelling advection. Therefore, the concentration profiles in the turbulence-dominated region are always smoothed out by turbulent advection mechanisms.

To conclude our analysis of wind effects on swimmer dynamics, we present orientation statistics. In particular, in Fig. 6 we show the behavior of $\langle p_x \rangle$ and $\langle p_z \rangle$ along the wall-normal direction, for all simulated cases. To correlate swimmer orientation with vertical migration and surfacing, we focus our attention on the upper portion of the flow domain, where the swimmers interact with wind-induced shear.

In the free-slip case (panels (a) and (d) in Fig. 6), $\langle p_x \rangle$ is always small while $\langle p_z \rangle$ increases with Ψ: It is clear that, even without wind forcing, turbulence can disrupt directional swimming for low gyrotaxis. A similar finding has been reported for floaters (Lovecchio et al., 2013; 2014). As gyrotaxis increases, bottom heaviness becomes predominant and allows swimmers to reach an equilibrium orientation in the direction opposite to gravity. In the co-current case (panels (b) and (e) in Fig. 6), weak (resp. strong) vertical swimming is observed for low (resp. high) gyrotaxis: For the Ψ_L case, this result indicates that local turbulent fluctuations are still strong enough to destabilize the directional motion of the swimmers, being $\Psi_L \cdot \tau^+_{K,max} \sim \mathcal{O}(10^{-1})$, and wind-induced shear seems to bring minor quantitative changes to the statistics; for the Ψ_H case, it indicates that cell motility is mainly determined by gravitaxis since gravitational acceleration is larger than fluid acceleration and $\Psi_H \cdot \tau^+_{K,max} \sim \mathcal{O}(10)$: In this limit, we always find $\langle p_z \rangle \simeq 1$. A less trivial behavior is observed for the Ψ_I case: Compared to the free-slip flow, significantly higher values of $\langle p_x \rangle$ associated to lower values of $\langle p_z \rangle$ are now observed within

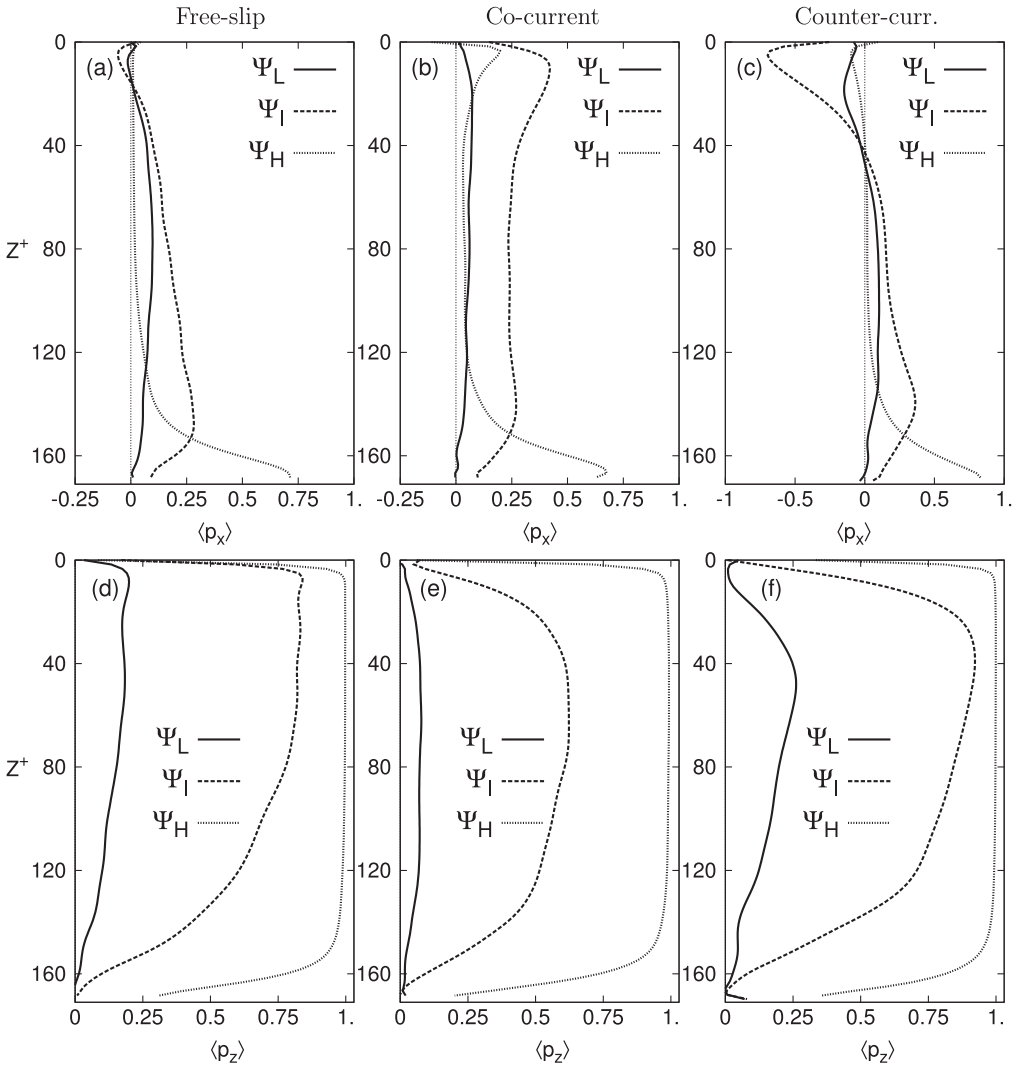

Fig. 6. Mean orientation of the swimmers, $\langle p_i \rangle$, along the wall-normal direction at varying gyrotaxis (Ψ_L: solid line, Ψ_I: dashed line, Ψ_H: dotted line). The free surface is located at $Z^+ = 0$. Panels refer to different wind conditions: (a), (d) free-slip surface; (b), (e) co-current wind; (c) and (f) counter-current wind.

the wind-induced high-shear surface layer. This is a mean-shear effect, which explains the non-monotonic behavior of $\langle p_x \rangle$ with Ψ and becomes more evident when $\Psi_I \cdot \tau^+_{K,max} \sim \mathcal{O}(1)$, namely when the re-orientation time of the swimmers is of the same order of the characteristic timescale of the small-scale (dissipative) turbulent eddies near the surface. Note that, once swimmers are able to trespass the high-shear region and reach the surface, they tend to align in the horizontal flow direction because wall-normal turbulent fluctuations decay to zero and swimmers are brought about only by the residual streamwise and spanwise fluid velocities (Lovecchio et al., 2014). In the counter-current case (panels (c) and (f) of Fig. 6, similar considerations can be made yet observing that the direction of wind produces a negative value of $\langle p_x \rangle$ near the surface, this value being maximum ($\langle p_x \rangle \simeq -0.7$) for $\Psi = \Psi_I$: In such situation, swimmers can move against the mean flow aided by wind forcing. We remark here that the non-monotonic behavior of $\langle p_x \rangle$ for $\Psi = \Psi_I$ is never observed near the wall, where both orientation components depend monotonically on the stability number. Such difference may be explained considering that, in this region of the flow, the Kolmogorov timescale is about one order of magnitude smaller than at the free surface: Therefore, the product $\Psi \cdot \tau^+_K$ is always order one (for $\Psi = \Psi_L$) or higher (for $\Psi \geq \Psi_I$) and gravitaxis tends to be more important than the ambient fluid turbulence.

The main conclusion that can be drawn from the concentration and orientation statistics examined in this section is that wind may have a significant damping effect on the surfacing of motile micro-organisms, which exhibit a narrower vertical spreading within the flow. Only organisms with high-enough gyrotaxis (namely strong-enough bottom-heaviness) can maintain their ability to swim upwards. A similar behavior was observed in the presence of temperature-induced stable stratification (Lovecchio et al., 2017), which appears to hinder surfacing and damp vertical mixing when temperature gradients are large enough to generate thermoclines and internal gravity waves. This effect may have important consequences for environmental processes such as spring phytoplankton bloom and growth, which are known to occur when turbulent mixing is sufficiently weak (Enriquez and Taylor, 2015).

4. Conclusions

In this study, we used direct numerical simulation and Lagrangian tracking to investigate the role of wind-induced shear on the vertical migration of gyrotactic swimmers in stably-stratified

free-surface turbulent channel flow. An extensive campaign of simulations was performed for different wind forcing and different re-orientation times of the swimmers, representative of common motile phytoplankton species and corresponding to different quickness in responding to external fluctuations. In the present physical configuration, the flow is driven by a constant pressure gradient. Simulations were run at shear Reynolds number $Re_\tau = 171$, and stability number $\Psi = 0.0113$, 0.113 and 1.3. In such flow, the flow structure near the free surface is strongly correlated with the active turbulent bursting phenomena that occur near the bottom wall (Calmet and Magnaudet, 2003; Nagaosa, 1999; Nagaosa and Hadler, 2003). Flow field modifications due to wind-induced shear are found to influence the ability of swimmers to reach the surface. In particular, we find that wind-induced shear modifies the vertical spread of the swimmers and their orientation with respect to the direction of gravity. For all gyrotactic re-orientation times considered in this study (spanning two orders of magnitude of the stability number), we observe a reduction of the cell rising speed and temporary confinement under the high-shear sub-surface layers: If re-orientation is fast, cells make it through the wind-induced shear region within the simulated time span and accumulate at the surface where high concentration levels may be reached; if re-orientation is slow, confinement lasts much longer because cells tend to align in the streamwise direction and lose their ability to swim upwards. We believe that these findings provide useful indications to parameterize the influence of wind forcing on the migration of motile algae (phytoplankton cells, in particular), and to develop models for predicting their dispersion inside large water bodies.

A future development of this study is the relative influence of wind-driven mixing and thermal stratification due to surface heating. This problem has been examined recently by Enriquez and Taylor (2015) with the aim of understanding how these physical drivers may trigger phytoplankton blooms. It would be interesting to examine the role of these drivers on phytoplankton vertical migration and surfacing. Thermal stratification in water bodies influences the exchange of heat, momentum and chemical species across the air–water interface by modifying the sub-surface turbulence characteristics. In particular, for strong enough surface heating, internal gravity waves (Ferrari and Wunsch, 2009; Hingsamer et al., 2014; Zonta et al., 2012) may arise due to the instability generated by lumps of denser (cold) fluid being lifted upwards into regions of lighter (warm) fluid by turbulence and subsequently driven downwards by buoyancy. These waves form near the free surface, correlate well with regions of the flow characterized by large temperature gradients and low mixing (thermoclines) (Taylor et al., 2005), and can act as thermal barrier for organic and inorganic matter (Lovecchio et al., 2017), with possible consequences on biogeochemical cycles, climate patterns and marine ecosystems, which are strongly sensitive to changes in marine biomass concentration (Acevedo-Trejos et al., 2015). Another interesting situation to investigate would be the motion of gryotactic swimmers in a wind-sheared flow subjected to an oscillating pressure gradient, which mimics a water layer in a shallow tidal channel or estuary (Kramer et al., 2010).

Acknowledgments

We gratefully acknowledge the CINECA supercomputing center (Bologna, Italy) and ISCRA Computing Initiative for generous allowance of computer resources. MM gratefully acknowledges the support of the Iranian government during her visit at the University of Udine and the generous support from ACRI through the 2016 Young Investigator Training Program.

References

Acevedo-Trejos, E., Brandt, G., Bruggeman, J., Merico, A., 2015. Mechanisms shaping size structure and functional diversity of phytoplankton communities in the ocean. Sci. Rep. 5, Article number: 8918.
Arrieta, J., Barreira, A., Tuavl, I., 2015. Microscale patches of nonmotile plankton. Phys. Rev. Lett. 114, 128102.
Calmet, I., Magnaudet, J., 2003. Statistical structure of high-reynolds-number turbulence close to the free surface of an open-channel flow. J. Fluid Mech. 474, 355–378.
Carrick, H.J., Aldridge, F.J., Schelske, C.L., 1993. Wind influences phytoplankton biomass and composition in a shallow, productive lake. Limnol. Oceanogr. 38, 1179–1192.
Chidambaran, N., Lakehal, D., Botto, L., Soldati, A., 2003. Mechanisms of particle deposition in a fully developed turbulent open channel flow. Phys. Fluids 15, 763–775.
Cressman, J.R., Davoudi, J., Goldburg, W.I., Schumacher, J., 2004. Eulerian and Lagrangian studies in surface flow turbulence. New J. Phys. 6, 53.
Croze, O.A., Sardina, G., Ahmed, M., Bees, M.A., Brandt, L., 2013. Dispersion of swimming algae in laminar and turbulent channel flows: consequences for photobioreactors. J. R. Soc. Interface 10 (81), 20121041.
De Lillo, F., Cencini, M., Boffetta, G., Santamaria, F., 2013. Geotropic tracers in turbulent flows: a proxy for fluid acceleration. J. Turbul. 14 (7), 24–33.
De Lillo, F., Cencini, M., Durham, W.M., Barry, W.M., Stocker, R., Climent, E., Boffetta, G., 2014. Turbulent fluid acceleration generates clusters of gyrotactic microorganisms. Phys. Rev. Lett. 112 (4), 044502.
Dekshenieks, M.M., Donaghay, P.L., Sullivan, J.M., Osborn, T.R., Rines, J., Twardowski, M.S., 2001. Temporal and spatial occurrence of thin phytoplankton layers in relation to physical processes. Mar. Ecol. Prog. Ser. 223, 61–71.
Durham, W.M., Climent, E., Barry, W.M., De Lillo, F., Boffetta, G., Cencini, M., Stocker, R., 2013. Wind stress measurements from the open ocean. J. Phys. Oceanogr. 26, 541–558.
Durham, W.M., Climent, E., Stocker, R., 2011. Gyrotaxis in a steady vortical flow. Phys. Rev. Lett. 106 (23), 238102.
Durham, W.M., Kessler, J.O., Stocker, R., 2009. Disruption of vertical motility by shear triggers formation of thin phytoplankton layers. Science 323 (5917), 1067–1070.
Durham, W.M., Stocker, R., 2012. Thin phytoplankton layers: characteristics, mechanisms, and consequences. Annu. Rev. Mar. Sci. 4, 177–207.
Enriquez, R.M., Taylor, J.R., 2015. Numerical simulations of the competition between wind-driven mixing and surface heating in triggering spring phytoplankton blooms. ICES J. Mar. Sci. 72, 1926–1941.
Ferrari, R., Wunsch, C., 2009. Ocean circulation kinetic energy: reservoirs, sources, and sinks. Annu. Rev. Fluid Mech. 41, 253–282.
Fouxon, I., Leshansky, A., 2015. Phytoplankton'S motion in turbulent ocean. Phys. Rev. E 92, 013017.
Ghorai, S., 2016. Gyrotactic trapping: a numerical study. Phys. Fluids 28, 041901.
Guasto, J.S., Rusconi, R., Stocker, R., 1992. Fluid mechanics of planktonic microorganisms. Annu. Rev. Fluid Mech. 44, 373–400.
Gutiérrez, P., Aumaître, S., 2016. Clustering of floaters on the free surface of a turbulent flow: an experimental study. Eur. J. Mech. B – Fluid 60, 24–32.
Hingsamer, P., Peeters, F., Hofmann, H., 2014. The consequences of internal waves for phytoplankton focusing on the distribution and production of planktothrix rubescens. PLoS One 9 (8), Article number: e104359.
Hoecker-Martínez, M.S., Smyth, W.D., 2012. Trapping of gyrotactic organisms in an unstable shear layer. Cont. Shelf Res. 36, 8–18.
Kessler, J.O., 1986. Individual and collective fluid dynamics of swimming cells. J. Fluid Mech. 173, 191–205.
Kramer, W., Clercx, H.J.H., Armenio, V., 2010. Turbulent oscillating channel flow subjected to a free-surface stress. Phys. Fluids 22, 095101.
Lovecchio, S., Marchioli, C., Soldati, A., 2013. Time persistence of floating particle clusters in free-surface turbulence. Phys. Rev. E 88, 033003.
Lovecchio, S., Zonta, F., Marchioli, C., Soldati, A., 2017. Thermal stratification hinders gyrotactic micro-organism rising in free-surface turbulence. Phys. Fluids 29, 053302.
Lovecchio, S., Zonta, F., Soldati, A., 2014. Influence of thermal stratification on the surfacing and clustering of floaters in free surface turbulence. Adv. Water Resour. 72, 22–31.
Lovecchio, S., Zonta, F., Soldati, A., 2015. Upscale energy transfer and flow topology in free surface turbulence. Phys. Rev. E 91, 033010.
Macías, D., Franks, P.J.S., Ohman, M.D., Landry, M.R., 2012. Modeling the effects of coastal wind- and wind-stress curl-driven upwellings on plankton dynamics in the Southern California current system. J. Mar. Syst. 94, 107–119.
Manela, A., Frankel, I., 2003. Generalized Taylor dispersion in suspensions of gyrotactic swimming micro-organisms. J. Fluid Mech. 490, 99–127.
McGillicuddy Jr., D.J., et al., 2007. Eddy/wind interactions stimulate extraordinary mid-ocean plankton blooms. Science 316, 1021–1026.
Moreno-Ostos, E., Cruz-Pizarro, L., Basanta, A., George, D.G., 2009. The influence of wind-induced mixing on the vertical distribution of buoyant and sinking phytoplankton species. Aquat. Ecol. 43, 271–284.
Nagaosa, R., 1999. Direct numerical simulation of vortex structures and turbulent scalar transfer across a free surface in a fully developed turbulence. Phys. Fluids 11, 1581–1595.
Nagaosa, R., Hadler, R.A., 2003. Statistical analysis of coherent vortices near a free surface in a fully developed turbulence. Phys. Fluids 15, 375–394.
Pedley, T.J., Kessler, J.O., 1990. A new continuum model for suspensions of gyrotactic micro-organisms. J. Fluid Mech. 212, 155–182.

Pedley, T.J., Kessler, J.O., 1992. Hydrodynamic phenomena in suspensions of swimming microorganisms. Annu. Rev. Fluid Mech. 24 (1), 313–358.
Pratt, K.R., True, A., Crimaldi, J.P., 2017. Turbulent clustering of initially well-mixed buoyant particles on a free-surface by Lagrangian coherent structures. Phys. Fluids 29, 075101.
Santamaria, F., De Lillo, F., Cencini, M., Boffetta, G., 2014. Gyrotactic trapping in laminar and turbulent Kolmogorov flow. Phys. Fluids 26 (11), 111901.
Steinbuck, J.V., Stacey, M.T., McManus, M.A., Cheriton, O.M., Ryan, J.P., 2009. Observations of turbulent mixing in a phytoplankton thin layer: implications for formation, maintenance, and breakdown. Limnol. Oceanogr. 54, 1353–1368.
Takagaki, N., Kurose, R., Kimura, A., Komori, S., 2016. Effect of Schmidt number on mass transfer across a sheared gas–liquid interface in a wind-driven turbulence. Sci. Rep. 6, 37059.
Taylor, J.R., Sutanu, S., Armenio, V., 2005. Large eddy simulation of stably stratified open channel flow. Phys. Fluids 17, 116602.
Thorn, G.J., Bearon, R.N., 2016. Transport of spherical gyrotactic organisms in general three-dimensional flow fields. Phys. Fluids 22, 041902.
Verhagen, J.H.G., 1994. Modeling phytoplankton patchiness under the influence of wind-driven currents in lakes. Limnol. Oceanogr. 39, 1551–1565.
Voth, G.A., Soldati, A., 2017. Anisotropic particles in turbulence. Annu. Rev. Fluid Mech. 49, 249–276.
Walker, J.W., Peirson, W.L., 2008. Measurement of gas transfer across wind-forced wavy air–water interfaces using laser-induced fluorescence. Exp. Fluids 44, 249–259.
Yelland, M., Taylor, P.K., 1996. Wind stress measurements from the open ocean. J. Phys. Oceanogr. 26, 541–558.
Zhan, C., Sardina, G., Lushi, E., Brandt, L., 2014. Accumulation of motile elongated micro-organisms in turbulence. J. Fluid Mech. 739, 22–36.
Zonta, F., Onorato, M., Soldati, A., 2012. Turbulence and internal waves in stably-stratified channel flow with temperature-dependent fluid properties. J. Fluid Mech. 697, 175–203.